

The Impacts of Climate Change on Autumn North Atlantic Midlatitude Cyclones

JING JIANG

Department of Atmospheric Sciences, Nanjing University, Nanjing, China

WILLIAM PERRIE

Fisheries and Oceans Canada, Bedford Institute of Oceanography, Dartmouth, and Dalhousie University, Halifax, Nova Scotia, Canada

(Manuscript received 22 July 2005, in final form 3 July 2006)

ABSTRACT

This study explores how midlatitude extratropical cyclone intensities, frequencies, and tracks can be modified under warming-induced conditions due to enhanced greenhouse gas (GHG) concentrations. Simulations were performed with the Canadian mesoscale compressible community (MC2) model driven by control and high CO₂ climate estimates from the Canadian Climate Centre model, the Second Generation Coupled Global Climate Model (CGCM2). CGCM2 simulations have effective CO₂ concentration forcing, following the Intergovernmental Panel on Climate Change (IPCC) IS92a scenario conditions, which define a near doubling of CO₂ concentrations by 2050 compared to the 1980s. The control and high CO₂ conditions were obtained from years 1975–94 and 2040–59 of CGCM2 simulations. For the northwest Atlantic, the CO₂-induced warming for this period (2040–59) varies from ~1°–2°C in the subtropics, near the main development region for Atlantic hurricanes, to ~1°C in the north. In simulations of northwest Atlantic storms, the net impact of this enhanced CO₂ scenario is to cause storms to increase in radius, with marginal tendencies to become more severe and to propagate faster (although not statistically significant), and for the mean storm tracks to shift slightly poleward.

1. Introduction

About half of all North Atlantic hurricanes have trajectories that track to the northwest Atlantic, becoming extratropical midlatitude storms, and about half of these experience extratropical transition (ET) and intensification (Hart and Evans 2001). In this study, we are concerned with possible climate change related to high-CO₂ environments, for all midlatitude storms, including extratropical transitioning hurricanes (ETs), as they propagate into the northwest Atlantic from their genesis areas in the North Atlantic tropical basin. Given the impact of these storms on coastal areas of North America due to heavy rain and high winds, and the large population densities living in these areas, the potential economic impacts may be significant.

In an overall sense, sea surface temperatures (SSTs)

over the North Atlantic Ocean tropical basin have experienced no significant trends over the past 50 years (Knutson et al. 1999), and SST-related trends in tropical cyclone intensities over this period have also not been observed (Landsea et al. 1996). However, an upward trend in SSTs is suggested over the past three decades in the *extratropical* North Atlantic by Trenberth (2005). Moreover, there is evidence that changes in cyclonic activity have occurred, related to *dynamical* changes in oceanic and atmospheric conditions (Gray 1984; Vitart et al. 1999; Goldenberg et al. 2001; Elsner et al. 2000). Lunkeit et al. (1998) showed that the North Atlantic storm track is enhanced (weakened) due to an increase (decrease) of baroclinicity by using a simplified global circulation model to investigate the greenhouse warming on Northern Hemisphere winter storm tracks. Carillo et al. (2000) found good correlation between winter storm tracks and zonal flow, and spatial displacements in the storm tracks correlate with jet stream shifts in the same direction.

Greenhouse gas (GHG)-induced climate change could modify the intensities of hurricanes, as well as

Corresponding author address: Dr. W. Perrie, Bedford Institute of Oceanography, P.O. Box 1006, 1 Challenger Drive, Dartmouth, NS B2Y 4A2, Canada.
E-mail: perriew@dfo-mpo.gc.ca

their frequencies and locations of occurrence. The Houghton et al. (2001) report on climate change suggests that regional frequencies of tropical cyclones may change, peak intensities may increase by 5%–10%, and precipitation rates may increase by 20%–30%. These conclusions are based on theoretical arguments concerning tropical cyclone potential intensity (Emanuel 1987; Holland 1997; Tonkin et al. 1997; Henderson-Sellers et al. 1998), as well as GCM studies (Bengtsson et al. 1995, 1996; Tsutsui and Kasahara 1996; Krishnamurti et al. 1998; Royer et al. 1998; Yoshimura et al. 1999; Sugi et al. 2002; Tsutsui 2002); regional climate model simulations of typhoons, driven by GCM fields (Walsh and Watterson 1997; Walsh and Katzfey 2000; Walsh and Ryan 2000; Walsh et al. 2004); and hurricane-model-climatology studies using GCM-derived thermodynamic and moisture environmental conditions (Knutson et al. 1998; Knutson and Tuleya 1999; 2004), including ocean model coupling (Knutson et al. 2001). Recent studies by Emanuel (2005) and Webster et al. (2005) confirm the suggestion that in the present climate, there is a 30-yr trend toward more frequent and intense hurricanes, although the role of global warming is not clear.

We are concerned with the possible impact of climate change on North Atlantic *extratropical* cyclones, as suggested by the second-generation model Coupled Global Climate Model (CGCM2) of the Canadian Centre for Climate Modelling and Analysis (CCCma), in simulations defined by the Intergovernmental Panel on Climate Change (IPCC) IS92a scenario conditions. This scenario uses effective greenhouse gas forcing fields corresponding to those observed from 1850 to 1990, with an assumed climate change corresponding to a CO₂ increase at a rate of 1% year⁻¹ thereafter until year 2100. CGCM2 simulations resulting from the IPCC IS92a scenario conditions suggest warming in the northwest Atlantic by about ~1°C. We are especially interested in examining possible changes in cyclone intensities, preferred locations and trajectories, vertical structures, and cyclone propagation speeds in the future climate scenario. Knippertz et al. (2000) analyzed outputs from the ECHAM4/Ocean Isopycnal Model (OPYC3) coupled ocean–atmosphere model, with transient GHG forcing according to the IPCC IS92a scenario and found that cyclone activity undergoes a pronounced northward and eastward shift over the northeast Atlantic, with a decrease in the number of weak cyclones and an increase in deep cyclones. Through analysis of indices of extratropical cyclone activity in winters, Paciorek et al. (2002) suggest that there is a recent increase in intense extratropical cyclone activity in the North Atlantic, in analysis of National Centers

for Environmental Prediction–National Center for Atmospheric Research (NCEP–NCAR) reanalysis data (Kalnay et al. 1996). Fischer-Bruns et al. (2005) use a coupled atmosphere–ocean model to simulate several centuries and detect a poleward shift in North Atlantic storm tracks, as well as an increase in cyclone activity, in climate change experiments.

Following Knutson and Tuleya (1999), we performed relatively high resolution storm simulations using the Canadian mesoscale compressible community (MC2) model driven by boundary conditions from the CGCM2 IS92a scenario outputs from the (i) present climate (represented in this study as 1975–94) and (ii) high CO₂ climate conditions (for 2040–59), when CO₂ levels are estimated to be approximately doubled (Boer et al. 2000a; Flato et al. 2000; Flato and Boer 2001). CGCM2 is a spectral model with a T32 triangular resolution of approximately 3.75° in latitude and longitude. Using MC2, we downscale all autumn (September–October) midlatitude storms for the present climate, and the high-CO₂ climate conditions. Lambert (2004) found that the CO₂-enhanced regime from the CGCM2 simulation gives greater numbers of the most intense storms in the North Atlantic, compared to the present climate. However, the CGCM2 resolution is too coarse to allow consideration of storm structure details.

In section 2, we describe the model setup for MC2 and the methodology for using the CGCM2 outputs as initial and lateral boundary conditions. Section 3 outlines the objective methodology used in selecting and tracking storms. Section 4 compares results from the MC2 simulations with those from CGCM2 and related datasets. Section 5 gives statistical analysis of the storm simulations, and section 6 presents conclusions.

2. The model

The MC2 atmospheric model is very versatile and has been successful in simulations of extratropical cyclones (Benoit et al. 1997; McTaggart-Cowan et al. 2001, 2003). MC2 is a state-of-the-art fully elastic nonhydrostatic model, using a semi-implicit semi-Lagrangian time scheme (Tanguay et al. 1990). This model solves the full Euler equations on a limited-area Cartesian domain, using a staggered grid with uniform horizontal and nonuniform vertical resolution, with time-dependent nesting of lateral boundary conditions. Orography is accommodated by using the Gal-Chen vertical coordinate, with higher resolution at lower levels. Over the sea, the MC2 interfacial fluxes of momentum and sensible and latent heat are calculated using Monin–Obukhov theory. Thus, air–sea fluxes are parameterized in terms of a bulk turbulent flux formulation, based on turbulent transfer coefficients depending

on empirical similarity functions and roughness lengths for wind speed, temperature, and humidity. In this paper, the model domain is 20.5°–65.25°N, 79.5°–29.75°W, which includes the northwest Atlantic and eastern North America continent, with 0.25° (~25 km) horizontal resolution and 30 vertical layers. The integration time step is 600 s. For extratropical cyclone simulations, we take initial conditions and boundary conditions from CGCM2 outputs.

3. Storm detection and methodology

Extratropical storms were selected from 20-yr datasets, as generated by CGCM2 simulations for 1975–94 and 2040–59, using an automated storm detection and tracking methodology to identify storm cases in the two 20-yr periods. These datasets are assumed representative of the control and climate change periods, respectively. Storms were specified in terms of local minima of sea level pressure (SLP). If there is a closed low pressure contour with central SLP less than 1005 mb, located in the region 25°–45°N, 80°–50°W, and if the SLP system has a lifetime of at least 24 h, the storm is considered a candidate for this study. Because we are only concerned with autumn storms that affect the midlatitude coast of North America, we consider only those storms that follow storm tracks oriented from southeast to northwest. This set of selection criteria results in a population of 72 autumn (September–October) storm cases in the present climate and 66 storm cases in the climate change scenario. Hart and Evans (2001) found that these months represent a large portion of the *extratropical* North Atlantic hurricane population. Thus, although we do not create an ensemble of storms, we do create a storm collection that resembles their climatology.

All storm cases were simulated using MC2, as motivated by the methodology of Knutson et al. (1998) and Knutson and Tuleya (1999), as described in section 1. Our simulations are located in the extratropical North Atlantic, whereas they are concerned with the tropical northwest Pacific. MC2 uses one-way nesting, with the lateral boundary conditions specified from CGCM2. The SSTs over the entire domain and the initial environmental conditions for each case are derived from CGCM2.

To determine whether differences between the families of storms simulated in the two climate scenarios are statistically different from each other, we employ the Student's t test. Assuming means (\bar{x}_1 , \bar{x}_2) and standard deviations (S_1 , S_2) of two group samples, which have sample sizes n_1 and n_2 separately, the t value can be calculated as follows:

$$t = \frac{\bar{x}_2 - \bar{x}_1}{\sqrt{S_1^2/n_1 + S_2^2/n_2}}.$$

For a given level of significance α and freedom degrees ν ($= n_1 + n_2 - 2$), if the absolute value of the t value is above the critical value t_{α} , the difference of means is significant at that level.

4. Storm case characteristics

A concern is comparisons of our control (present climate) simulations of storm tracks and intensities with analogous North Atlantic storm climatologies for the period 1975–94. In this section, we compare our results with 40-yr European Centre for Medium Range Weather Forecasting (ECMWF) Re-Analysis (ERA-40) 6-hourly SLP analysis data (www.ecmwf.int/research/era) with 2.5° resolution, with the CGCM2 simulation results with T32 (about 3.75°) resolution, and with National Hurricane Center (NHC) best-track data.

a. Spatial storm frequencies

Figure 1a presents the SLP-derived spatial storm-track frequency distribution, for the period 1975–94, using the MC2 mesoscale storm simulations with boundary and initial conditions defined from the CGCM2 fields. This distribution is determined by counting the number of storm tracks that passed through each 2.5° × 2.5° latitude–longitude box in autumn months (September and October) and averaged over 20 years (more detailed storm tracks can be seen in Fig. 5a). The dominant North Atlantic storm-track region is evident. Comparable results for CGCM2 data are given in Fig. 1b, again reflecting the dominant North Atlantic storm tracks. Corresponding ERA-40 and NHC results are presented in Figs. 1c and 1d, respectively, and give similar results.

Figures 1a–d show that the highest frequency concentration of storm events tends to occur near the east coast of North America. This corresponds to the tendency for most storms to move poleward in a curved pathway around the periphery of the subtropical North Atlantic high. The axis of maximum storm events occupies a southwest-to-northeast directional orientation with some variation in distance from the coast of North America, and most storms tracks tend to move poleward following this orientation. The results from our MC2 simulations (Fig. 1a) exhibit dominant axes of maximum storm events that are approximately parallel to the coastline. By comparison, the CGCM2 (Fig. 1b) data suggest a tendency for more storms to occur at

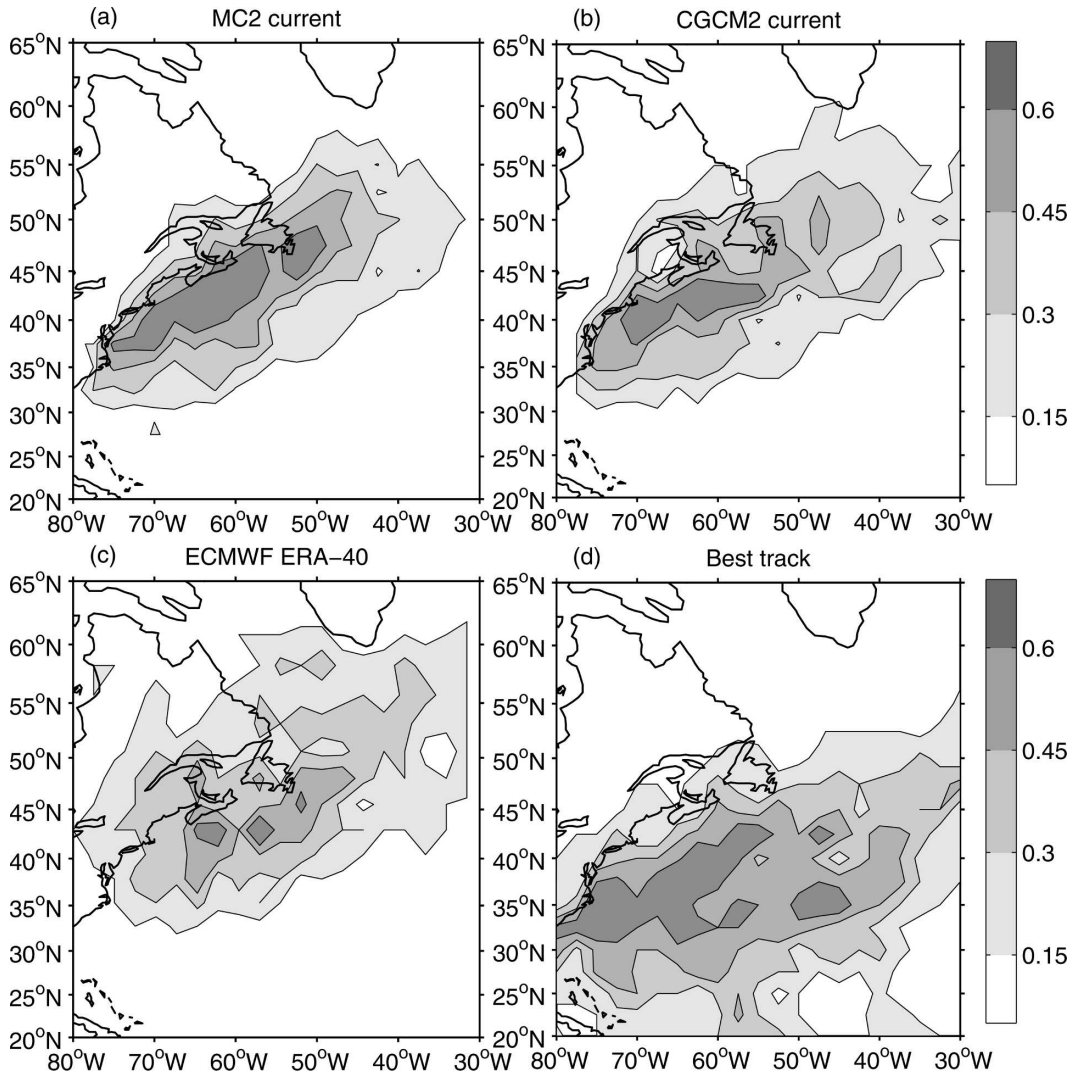


FIG. 1. Frequencies of storm tracks determined from SLP for simulations by (a) MC2, (b) CGCM2, (c) ERA-40 data, and (d) NHC best-track data for July to November during 1975–94.

latitude 40°N, although the axis of most storm events tends to be almost the same as in the MC2 data. The spatial distributions of the ERA-40 and NHC data (Figs. 1c–d) are similar to the MC2 data (Fig. 1a), although farther from the North American coast.

Figures 2a and 2b compare frequency distributions for maximum 10-m winds (U_{10}) from our MC2-derived control storm simulations (Fig. 1a) with kinematically analyzed NCEP winds by Swail and Cox (2000). The overall distribution of maximum winds in our simulations (Fig. 2a) is comparable to the SLP-based storm frequency distribution (Fig. 1a). By comparison, the kinematically enhanced NCEP maximum wind distribution (Fig. 2b) is similar to that resulting from the MC2 simulations. For discussion on how realistic the kine-

atically analyzed NCEP winds are, see Swail and Cox (2000).

The degree of similarity shown between our model-generated climatologies and reanalysis datasets in Figs. 1–2 is similar to that achieved by Knutson and Tuleya (1999) in comparisons between their model-simulated climatologies and NCEP reanalysis data. The spatial correlation between the storm frequency distributions from MC2 (Fig. 1a) and ERA-40 reanalysis data (Fig. 1b) is 0.77. For MC2 winds and kinematically analyzed NCEP winds (Figs. 2a and 2b), the spatial correlation is 0.81. Both correlations are statistically significant at the 0.001 level. Thus, the MC2–CGCM2 model simulations achieve an overall representation of the reanalysis data.

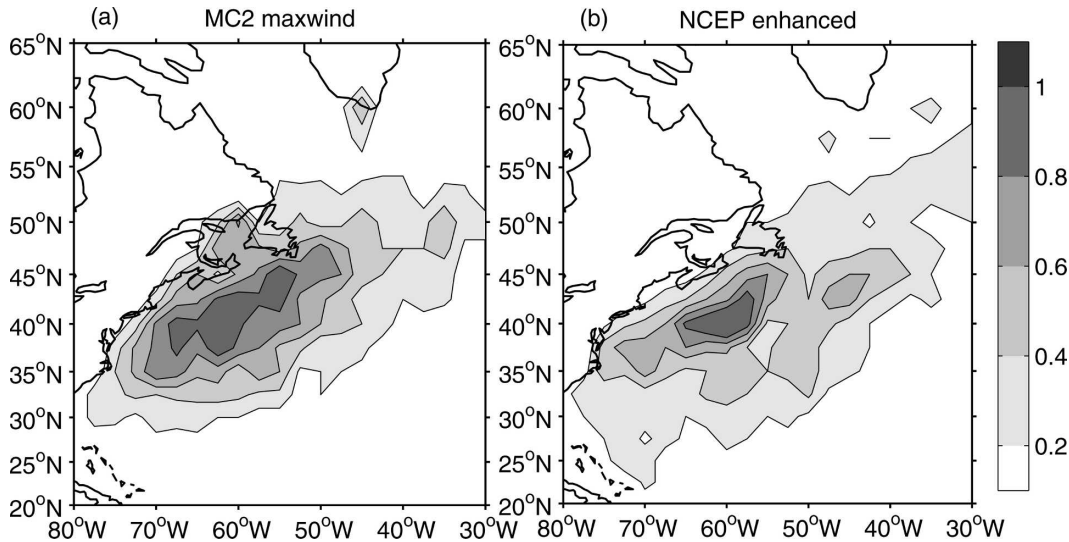


FIG. 2. As in Fig. 1 but for frequencies of storm tracks determined from maximum wind speeds in simulations by (a) MC2 and (b) kinematically enhanced NCEP wind fields by Swail and Cox (2000).

b. Storm intensities

Estimates for the SLP-derived storm intensity population distributions are shown in Fig. 3. This shows that MC2 simulations have the largest representation of the very severe storms (<975 hPa) and the NHC data contain the largest number of the most intense storms (<945 hPa), whereas the other two datasets (CGCM2 and ERA-40) suggest fewer storms in this category. In the largest segment of the distribution, the 905–985-hPa interval, the portion of storms in the MC2–CGCM2 simulations is about 74%, which is comparable to 72%

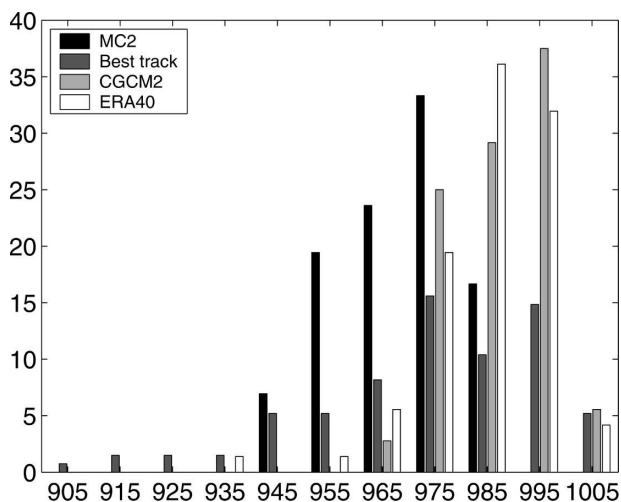


FIG. 3. Frequency of minimum SLP for storms simulated by MC2, CGCM2, and ERA-40, and NHC best-track data, expressed in units of %.

for the NHC dataset, although higher than the corresponding results, ~56% in the CGCM2 dataset and ~60% in the ERA-40 dataset. The MC2–CGCM2 simulations clearly suggest more very severe storms than either the CGCM2 or ERA-40 storm datasets. They are also consistent with the suggestion by Hart and Evans (2001) that coarse-resolution reanalysis data often underestimate the intensity of tropical cyclones and that the error in estimated intensity changes occurring in associated extratropical hurricanes can be large.

Figures 4a and 4b compare the maximum winds of storms from the MC2–CGCM2 storm simulations to NHC best-track data. Results are shown for distributions of maximum absolute U_{10} for the control and also the corresponding climate change storm populations. The three distributions are similar, although the winds simulated by MC2 are weaker than NHC winds in the most intense cyclones. For storms with winds above 25 m s^{-1} , the frequency of storm cases increases from 68% to 74% in the climate change scenario compared to the control distribution, suggesting a small intensification in the overall population. It is not significant by the Kolmogorov–Smirnov two-sample test (KS test). Corroborating results for minimum SLP are given in Fig. 4c, comparing the control dataset to the corresponding climate change storm population. Changes in the SLP distributions are also not significant by the KS test.

c. Storm tracks

The storm tracks from the mesoscale MC2 model simulations for each of the storms selected for the present and climate change simulations are shown in

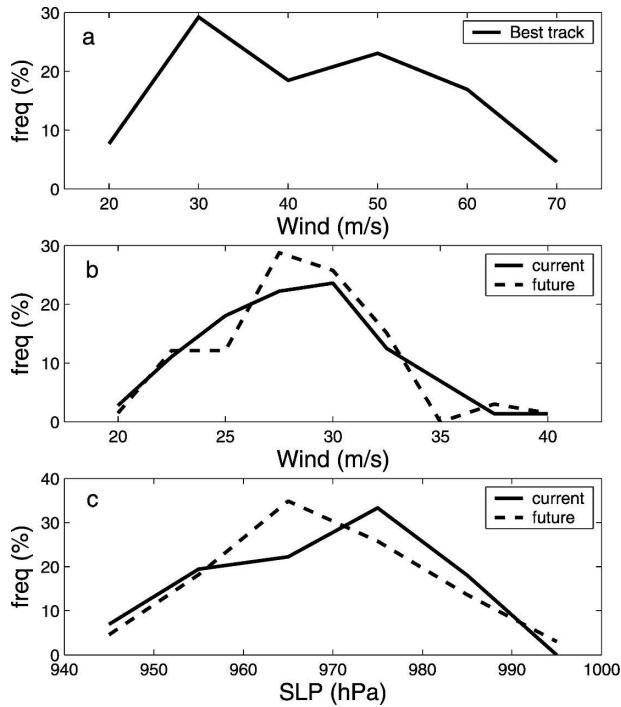


FIG. 4. (a) Maximum winds U_{10} from NHC best-track data and for (b) MC2-derived maximum U_{10} for current (1975–94) and climate change scenario (2040–59) storms and (c) MC2-derived SLP for current and climate change scenario.

Figs. 5a and 5b, respectively. These reflect the dominant northeastward trend for storm tracks in the North Atlantic. Considerable noise seems apparent in the distributions, resulting from the variability in the data. A

very slight systematic poleward shift is suggested, moving the mean storm track toward the coast under climate change conditions, as shown from a cluster analysis (using “nearest distance clustering”) for these two datasets in Fig. 6. For comparison, we also present the corresponding storm tracks from the CGCM2 climate model (Fig. 6). Overall, the CGCM2 mean storm tracks are similar to the MC2 mean storm tracks, comparing the control and climate change datasets.

For the present and climate change scenarios, the mean storm tracks for MC2 results are parallel with a slight tendency for the latter to move poleward, placing them on the order of about 200 km closer to the coastline. Similar results are obtained from the CGCM2 dataset, as was also noted by Fyfe (2003) from the CGCM2 simulation of climate change in the Southern Hemisphere. This is perhaps a result of changes in the steering flow (mean climatological flow) in the climate change scenario, compared to the control climate simulation. Figures 7a and 7b show the climatological-mean westerly wind speed in autumn at 250 hPa from the present and climate change scenario of CGCM2. It is evident that the upper westerly jet stream in the climate change scenario is somewhat stronger and farther north than that in the present climate. The corresponding geopotential height at 850 hPa from CGCM2 in the current and the climate change scenarios are shown in Figs. 7c and 7d. These plots show that, in the high- CO_2 scenario, the subtropical high is stronger and extends westward and northward and, as a result, storms also tend to be closer to the North American coast than in

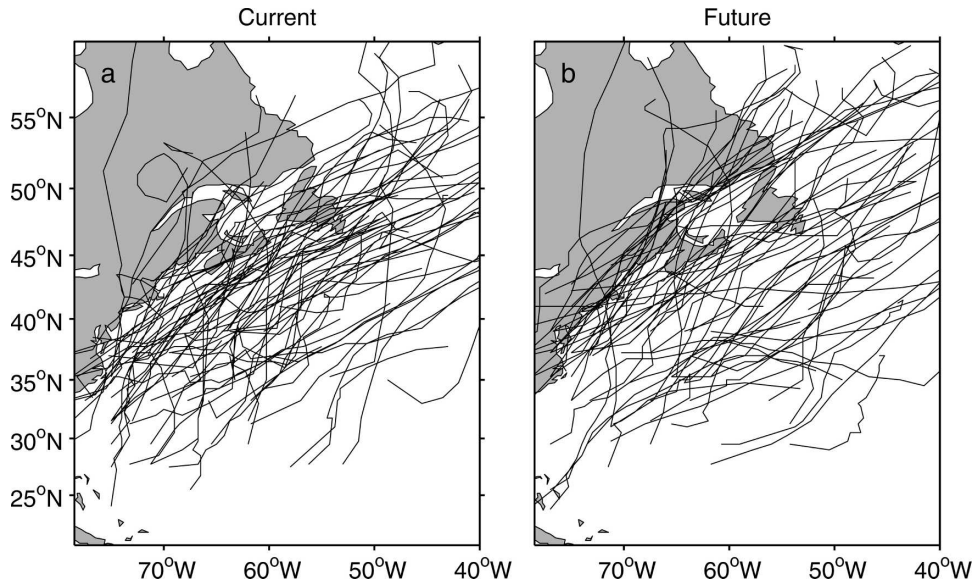


FIG. 5. Storm tracks (position every 6 h) for (a) the control and (b) climate change case studies using the MC2 mesoscale atmospheric model.

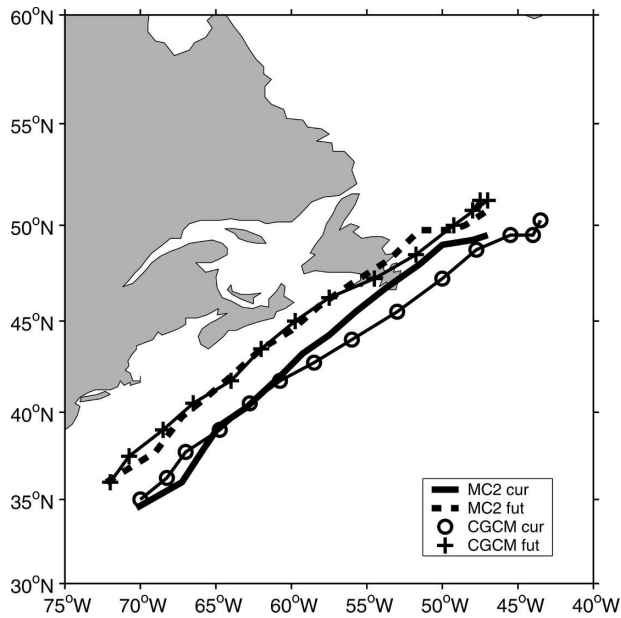


FIG. 6. As in Fig. 5 but using cluster analysis of the storm tracks to generate mean storm tracks (based on 6-hourly positions) for the control and climate change scenario storm populations, showing mesoscale MC2 model results in comparison with CGCM2 climate model storm simulations.

the present climate. Overall, the mean tracks for the MC2 simulations are slightly more poleward than those of the CGCM2 dataset, for both present and climate change scenarios. This result differs from that of Knutson and Tuleya (1999), who found more poleward tracks for a low-resolution global model compared to a nested high-resolution regional model. They suggested that the more poleward climate model results in their study may result from the much larger size of climate model storms, compared to mesoscale simulations.

d. Storm propagation speeds

In addition to storm tracks and intensities, we also consider storm propagation, because storms and ocean dynamics are coupled and extratropical hurricanes tend to propagate faster than tropical hurricanes. Moreover, they are influenced by the environmental fields through which they move, including the air–sea fluxes and wind-generated surface waves, which respond resonantly to differing storm speeds and atmospheric forcing wind and pressure fields. Figure 8 shows that the storms in the climate change scenario have an average propagation speed faster than that of the present climate, consistent with upper steering streamflow in Fig. 7. In this calculation, storm propagation speed is estimated as an average for the duration of each storm life cycle. Compared to an average storm propagation speed of

$0.37^{\circ} \text{ h}^{-1}$, for current control climate, the average propagation speed is $0.42^{\circ} \text{ h}^{-1}$ in the future climate scenario. This corresponds to an increase from about 11.4 m s^{-1} to about 12.9 m s^{-1} , which is about 13.5%. Tests by Moon et al. (2004) suggest that an increase in storm speed from 5 to 10 m s^{-1} can lead to more than 25% increase in maximum wave heights.

5. Storm structure

More detailed storm structure estimates are available from the MC2 simulations than are possible for the storms occurring in the CGCM2 outputs, comparing present and climate change scenario storm populations. We consider the detailed storm structure, for example, constructing composite storm winds by averaging the wind on storms over 100×100 grids ($25^{\circ} \times 25^{\circ}$) about the storm centers. For this calculation storm centers are specified by the minimum SLP.

a. Horizontal wind distribution

To explore the spatial storm distributions, Figs. 9a and 9b present composite two-dimensional spatial distributions of 1000-hPa wind speeds for storms of the present and climate change scenario populations, respectively. As expected, in either case the wind speed distributions are not symmetric about the storm center. In the present climate (Fig. 9a), the maximum wind region occurs in the right forward quadrant relative to the orientation of the storm propagation direction, for example, shown in the mean storm tracks in Fig. 6. Note that the storm propagation direction is to the northeast in Fig. 9. The winds on the left side are notably weaker, although a secondary maximum does occur. In the climate change scenario result (Fig. 9b), the secondary left-side maximum in wind increases slightly in spatial extent, and stronger winds tend to occur toward the front of the storm, not only the right side relative to the storm propagation direction but also on the left side. Not only is the region of highest winds around the storm center enlarged in the future climate relative to the present climate, but the overall horizontal structure of the storm is increased in the climate change scenario composite plot.

The distributions presented in Figs. 9a–b are composites of all of the MC2 storm simulations for present and climate change conditions, respectively. There is a high level of noise in the corresponding distributions because of the variability of the data. As a further illustration of the wind profiles, Figs. 10a and 10b give the variations in radial-averaged wind speeds with respect to the storm center for MC2 and CGCM2 simu-

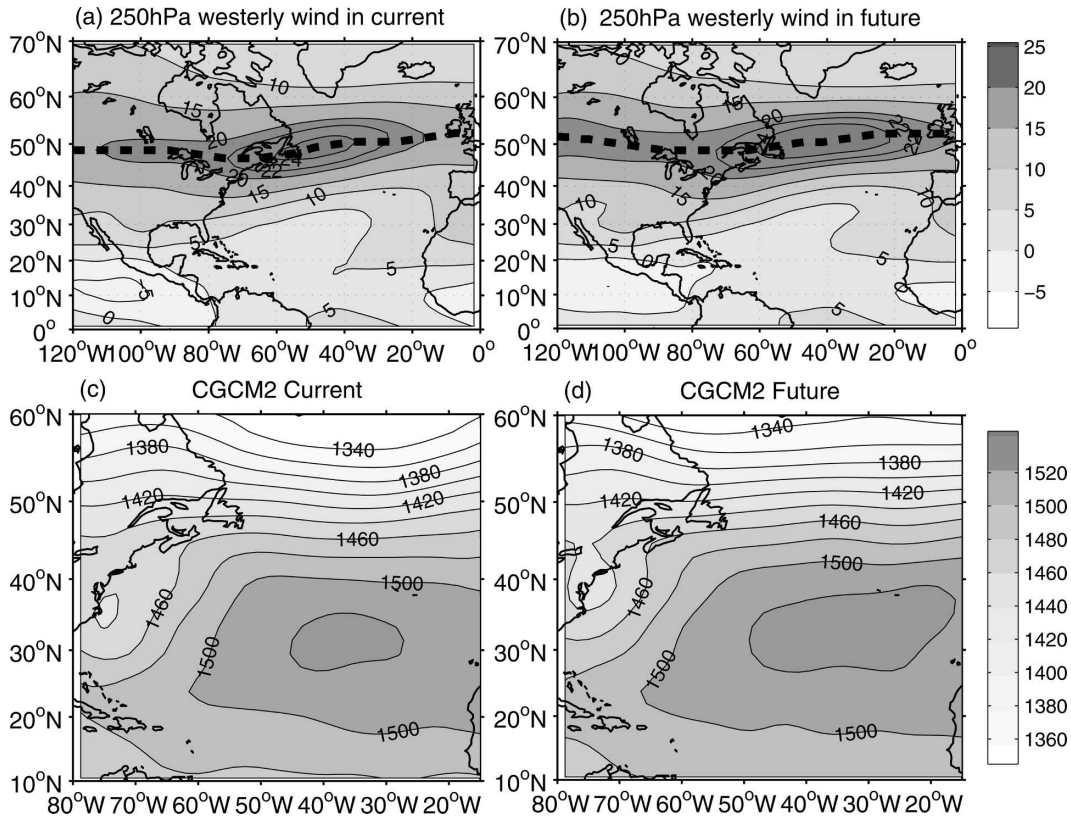


FIG. 7. Climatological-mean maps from CGCM2 for 250-hPa westerly wind speed in autumn for (a) present climate and (b) climate change scenario (unit: m s^{-1}), and geopotential height at 850 hPa from CGCM2 in (c) current and (d) future climate (unit: gpm).

lations, respectively. In these figures, the bold lines are the means of the entire population of storms for present and climate change families, and the thin lines represent the mean ± 1 standard deviations. We show that

there is little change in maximum winds in the future climate change scenario compared to the present climate for either MC2 or CGCM2 datasets. Overall the CGCM2 wind profile changes are similar to those of the MC2 simulations (Fig. 11), comparing control and climate change datasets. However, the tendency for the overall storm structure to broaden spatially is evident, as indicated by an increased radial distribution from the storm center, in both the MC2 and the CGCM2 profiles. In the outer regions of the storm, winds for the MC2 climate change scenario are significantly stronger (at 10% significance level by the Student's t test) than corresponding winds in the present climate: the 14 m s^{-1} radius increases by about 25%. However, changes in the CGCM2 results are not statistically significant.

b. Vertical wind distribution

To explore the vertical distribution of the composite storm structures, we consider cross sections passing through the storm centers and transecting the maximum wind centers, as indicated in Figs. 9a–b. Vertical wind profiles are shown in Figs. 12a and 12b for the current climate and the future climate change scenario,

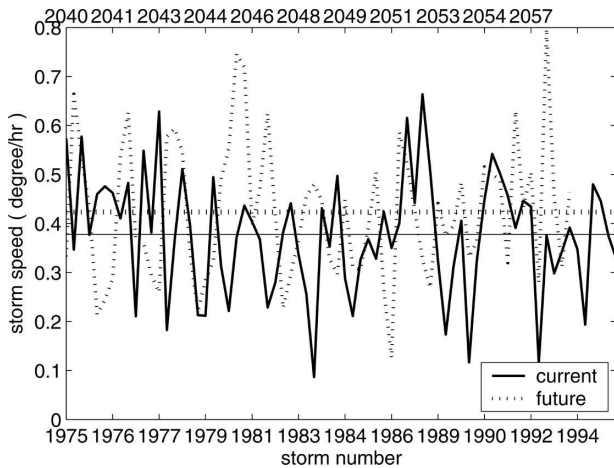


FIG. 8. The storm propagation speed in the current (solid line) and future (dashed line) climate (unit: degrees hr^{-1}) as a function of year, estimated as average speed during the storm life cycle.

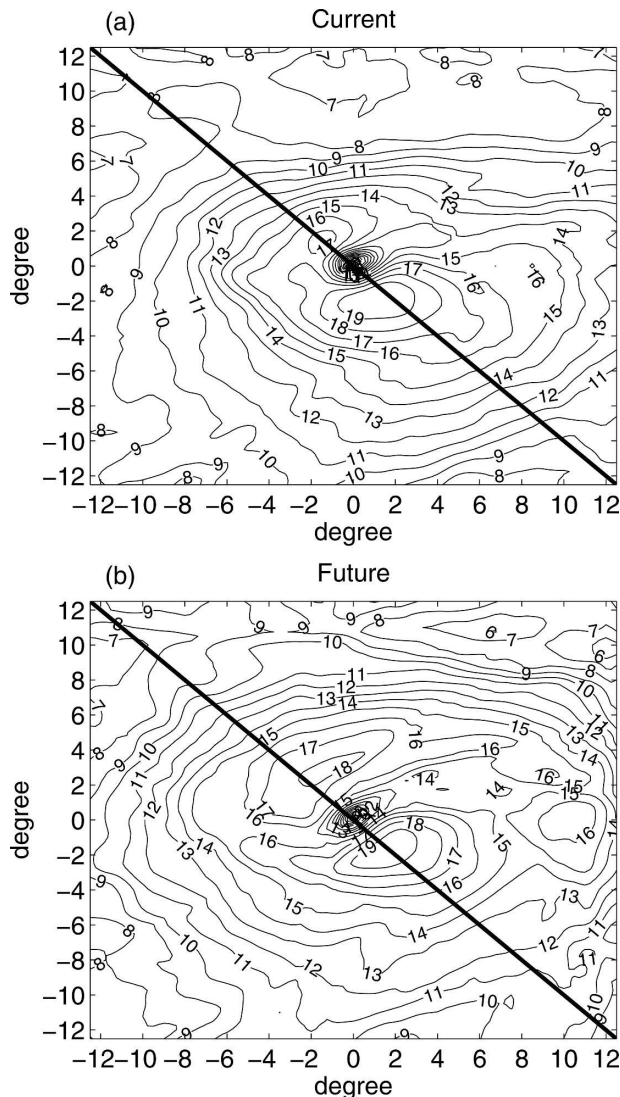


FIG. 9. Spatial distributions for 1000-hPa wind speed averaged on all storms over $25^\circ \times 25^\circ$ near the storm center, simulated by MC2. Diagonal lines represent location of vertical transects in Figs. 12–14.

respectively. Differences (future minus present) are presented in Fig. 12c, and vertical temperature profiles in Fig. 13. In Figs. 12c and 13, the shaded areas indicate statistical significance at the 5% level, according to the standard Student's *t* test. In Figs. 12a,b the composites are defined as the mean of all cases at the time of maximum intensity (from 6-hourly data) with all fields taken relative to the storm center. Composite cross sections are centered at the latitude of the storm, with the horizontal transect distance expressed in longitude degree units and the vertical axis in terms of pressure (hPa).

The wind distributions (Figs. 12a,b) are highly asym-

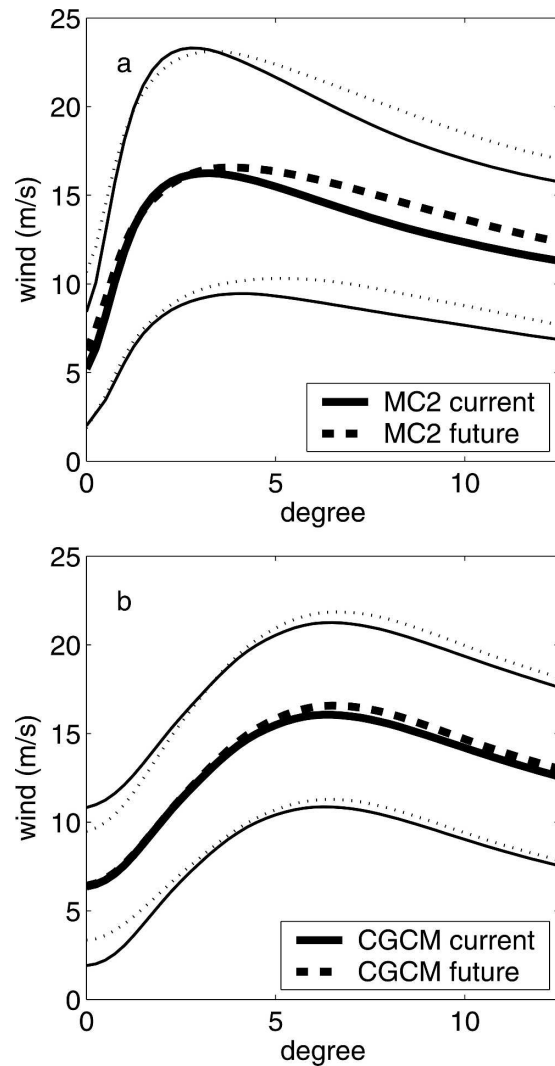


FIG. 10. As in Figs. 9a,b but for average (bold solid and dashed lines) and mean ± 1 standard deviation (thin solid and dashed lines) of wind around the storm center for all storms simulated by (a) MC2 and (b) CGCM2. The *x* axis is in units of degrees longitude.

metric with marked differences in the left and right sides of the composite storm structure. While the right side of the storm maintains a relatively high degree of uniformity as one goes from the upper limit of the atmospheric boundary layer to the top of the troposphere, particularly for the present climate simulation, the left side of the storm structure is quite variable with height, for either the present or the climate change scenario simulations. In the current climate (Fig. 12a), maximal winds tend to occur throughout most of the troposphere from the boundary layer upward at about 2° distance (~ 200 km) to the right side of the storm, with the winds at different levels having almost the

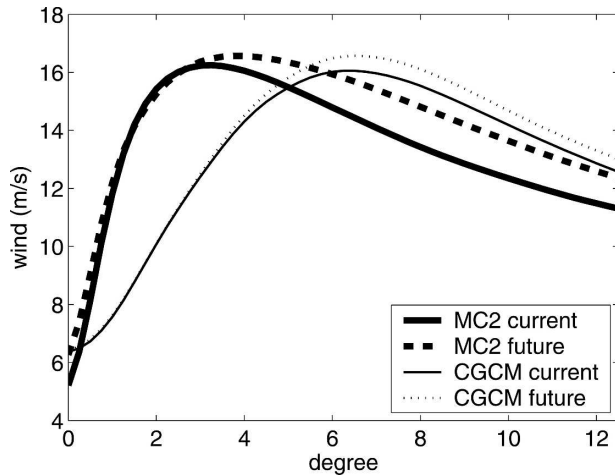


FIG. 11. As in Figs. 9a,b but for average of wind around the storm center for MC2 and CGCM2 data.

same speed. A secondary, more distant, high wind upper-level region occurs near the top of the troposphere at about 200 hPa to the left side of storm center, and a notably weaker region of high winds occurs about 2° distance (~ 200 km) to the left of the storm center in lower-tropospheric levels near the surface, as also shown in the 1000-hPa wind field in Fig. 9a.

In the climate change scenario simulation (Fig. 12b), the maximum wind is slightly stronger than that estimated for the current climate (Fig. 12a), although still about 2° distance to the right of the storm center. A peak in the maximum wind zone occurs at about 500 hPa. The high wind region at lower levels within the boundary layer at about 2° distance to the left of storm is also stronger than that exhibited in the current climate. The distant high wind upper-level region, on the left side of the storm near the top of the troposphere (~ 200 hPa), is considerably weaker than the result from the present climate simulation (Fig. 12a). Thus, there is weaker wind shear on the left side of the storm, perhaps explaining why the storm tracks in the climate change scenario tend to move poleward, slightly closer to the North American coast. The wind field difference (Fig. 12c) again suggests the existence of significantly higher winds in the upper-level region to the right of the storm center, and also to the lower left of the storm center, in the climate change scenario compared to the present climate.

c. Vertical temperature distribution

In an overall global sense, temperature tends to be warmer in the future climate scenario than in the present climate. In magnitude, in terms of vertical transects (defined in Figs. 9a,b), the future climate

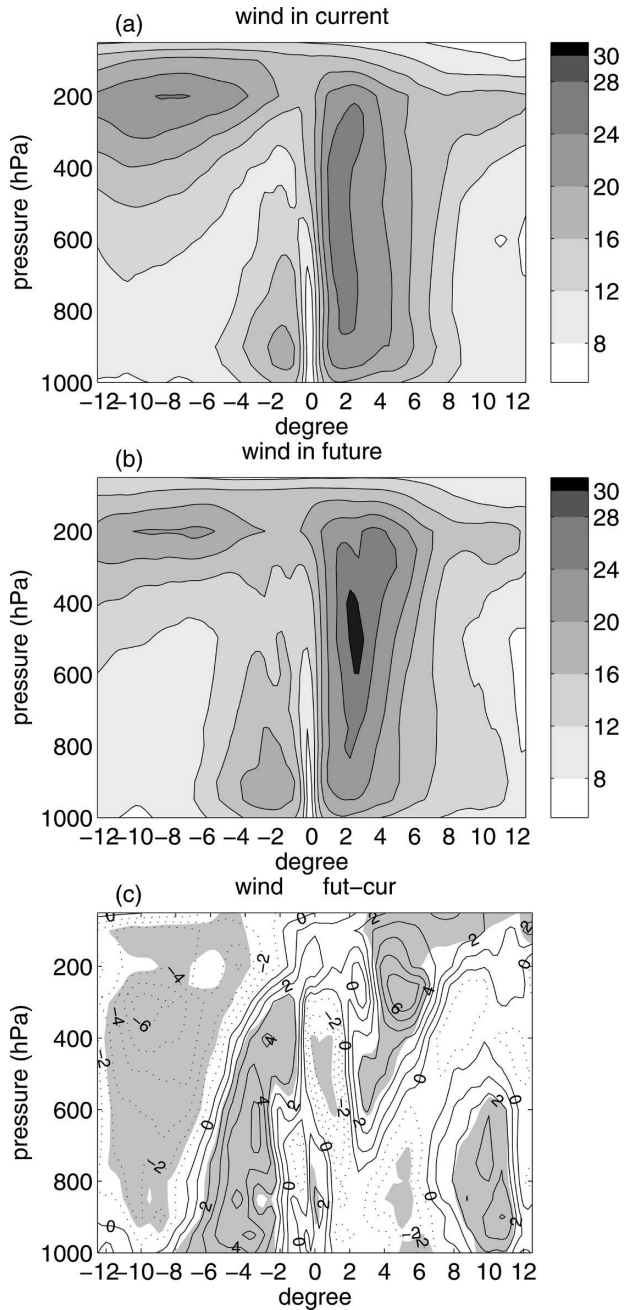


FIG. 12. Vertical wind profiles along transects passing through the storm center and the region of maximum winds, as indicated in Figs. 9a,b, for (a) current climate, (b) future climate, and (c) the difference (future minus current), where the shaded area indicates statistical significance at the 5% level.

change scenario is about 1°C warmer at low levels and generally more than 2°C warmer in the upper troposphere. According to the Student's t test, all of these warming trends in the troposphere are significant (at the 5% significance level). This is shown in Fig. 13. The

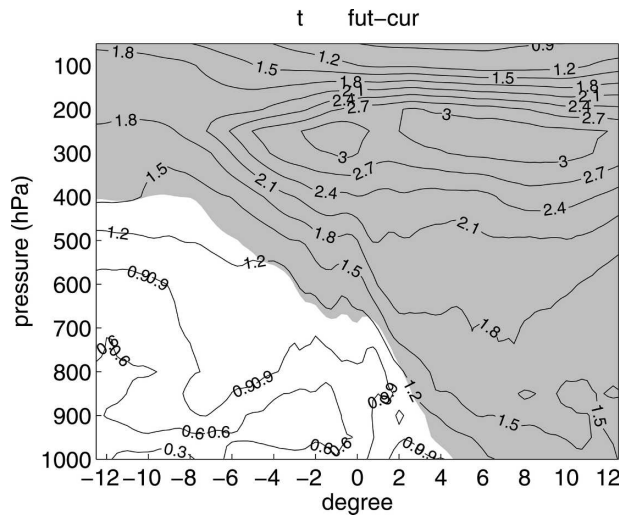


FIG. 13. As in Fig. 12c but for difference of vertical temperature profiles on transects in Figs. 9a,b centered on the storm. Abscissa is in units of degrees longitude; shading indicates areas of statistically significant changes at the 5% level.

warmest regions (larger than 3°C) are located in the upper part of the troposphere near 250 hPa, near the storm center and also to the right of the storm center. Differences in temperature are partially reflective of the environment in the current climate, compared to that of the climate change scenario. Following Knutson and Tuleya (1999), we remove the average vertical variation (relative to a $25^{\circ} \times 25^{\circ}$ domain centered on the storm) from the temperature profiles and obtain temperature anomalies at each pressure level for the present climate and climate change scenario (Figs. 14a and 14b) and the anomaly difference profile (Fig. 14c). The resulting anomaly profiles for present climate and climate change scenario are very similar, with the anomaly difference profile suggesting a slight ($<0.6^{\circ}$) warming anomaly in the boundary layer and upper troposphere to the right of the storm center, and slight cooling ($<0.6^{\circ}$) to the left of the storm center.

From Fig. 12c, the wind speed difference suggests an upward displacement in the height of the storm's upper level, as does the temperature anomaly difference from Fig. 14c, although it is not statistically significant (according to the Student's t test). These processes imply a slight increase in vertical depth of the storm. However, the vertical model resolution near the tropopause is about 2 km, which is too coarse to fully resolve this feature. Moreover, in terms of storm-related damage, the horizontal radius of maximum winds, shown in Figs. 9 and 11, is more important than the vertical depth of the storm, because low-level winds have a direct impact on society.

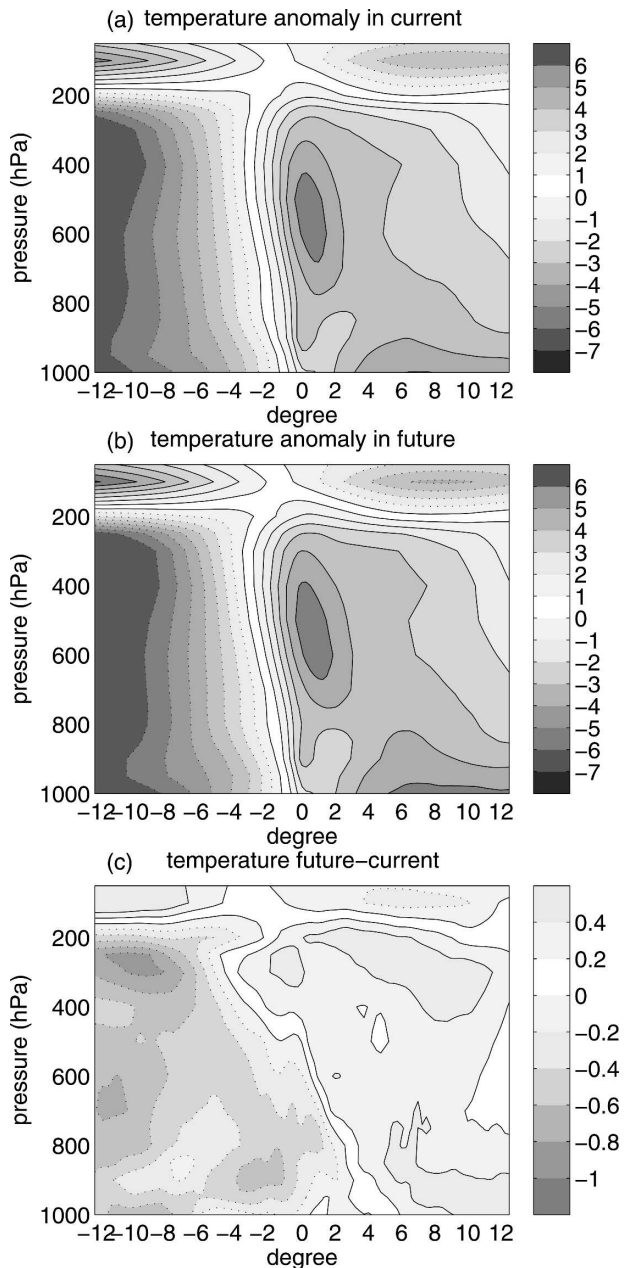


FIG. 14. As in Fig. 12 but for vertical temperature anomaly profiles on transects in Figs. 9a,b relative to the average over a $25^{\circ} \times 25^{\circ}$ domain centered on the storm: (a) current climate, (b) future climate, and (c) the difference.

d. Maximum horizontal winds

As a further representation of the wind distribution about the storm center, we consider the location of the maximum surface winds (V_{max}) relative to the storm center (Figs. 15). In this figure we use the hourly V_{max} following each storm track during the storm life cycle. Figure 6 showed that the storm tracks tend to move

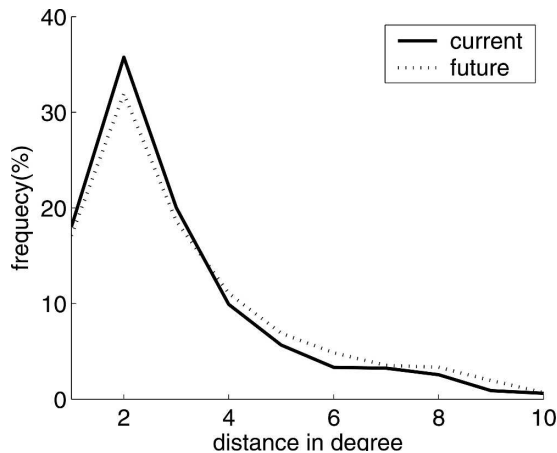


FIG. 15. Distance of the maximum wind location relative to the storm center.

poleward, moving closer to the coast in the climate change scenario, relative to the present climate.

Figure 15 gives the frequency distribution (for V_{\max} relative to the storm center) as a function of horizontal distance from the storm center, expressed in units of longitude degrees. This result suggests that the most prevalent occurrence of V_{\max} is at about 2° longitude (~ 200 km) from the storm center, for both the present climate and the climate change scenario. Although the peak for V_{\max} frequency is slightly smaller in the climate change scenario than in the present climate, the reduction in maximum wind speed with increasing distance from the storm center is slightly less rapid in the climate change scenario than in the present climate. This is also indicated by the enlarged horizontal storm structure suggested in Figs. 9 and 11, in the climate change scenario.

6. Conclusions

We have investigated the possible influence of climate change, represented by high- CO_2 conditions obtained from the Canadian Climate Centre CGCM2 model following the IPCC IS92a scenario, on midlatitude northwest Atlantic storms. Using automatic storm detection criteria based on sea level pressure (SLP), we selected storms from the present climate, represented by 1975–94, and also from the climate change scenario, represented by 2040–59. These cases were rerun with a mesoscale atmospheric model (MC2) at a relatively high horizontal resolution (0.25°). Compared to present storm climatology, for example, CGCM2 model outputs, ERA-40 data, and NHC best-track data, the storm intensities simulated by MC2 are shown to be representative.

Large-scale changes in environmental conditions are noted in comparing present and climate change scenarios: a warming of less than 1.0°C for the sea surface, less than 1.5°C for the lower troposphere, and about twice as much ($\sim 3^\circ\text{C}$) for the upper troposphere. Even though these seem like rather significant environmental changes, the mesoscale (MC2) simulations of storms in the climate change scenario tend to have about the same intensities as those of the present climate, in terms of either minimum sea level pressure or maximum wind speeds (V_{\max}). However, differences in their spatial and structural distributions are suggested. In the climate change scenario simulations, storms tend to exhibit larger horizontal extents than those in the present climate. Consideration of composite storm structures suggests that high winds occur at greater radii from the storm center, with the radius of 14 m s^{-1} winds increasing by about 25%. In terms of composite vertical structure, the climate change scenario simulations suggest that the maximum wind is slightly weaker at low tropospheric levels and relatively stronger winds occur in the mid to high troposphere, with maximum winds exceeding those for the present climate simulations. Moreover, the composite storm structure of the climate change scenario tends to penetrate slightly higher into upper troposphere than that of the present climate, which is qualitatively similar to the change noted by Knutson and Tuleya (1999).

A notable feature of the present study is the comparatively high resolution (0.25°) used in the storm region, relative to previous studies of midlatitude and high-latitude storms in climate change scenarios, based on global (GCM) models. Compared with the present climate, the storm tracks in the climate change scenario show a tendency to move slightly poleward nearer to the North Atlantic coast in both MC2 and CGCM2 simulations (Fig. 6). Moreover, the use of coarse-resolution GCMs may also lead to lower than observed storm intensities, and possibly lower sensitivity of storm intensities to climate warming, as compared to higher-resolution mesoscale models (although no statistically significant changes were found in this study). Storms in the climate change scenario also show a tendency to propagate faster. This may have an impact on their role as drivers of ocean waves and related surface currents.

The methodology applied here allows consideration of GCM results, regarding possible changes in storm frequencies, in future climate change scenarios. By using a mesoscale model (MC2), we are able to estimate the storm structure and to study the mechanisms related to changes in storm characteristics. A concern is that our neglect of ocean coupling effects may produce overestimates in storm intensities. Such ocean coupling

effects depend strongly on details for each individual storm, such as mixed layer depth and air–sea fluxes, which can vary in time and space through a storm’s life cycle (Perrie et al. 2004; Ren et al. 2004). In ongoing research, we hope to consider the impacts of the ocean surface and ocean coupling effects, including the ocean mixed layer depth and air–sea fluxes.

Acknowledgments. Support for this research comes from the Canadian Panel on Energy Research and Development (PERD—Offshore Environmental Factors Program), ONR and NOAA through the Gulf of Maine Ocean Observing System (GoMOOS), and the Southeast Universities Research Association Coastal Ocean Observing and Prediction program (SCOOP).

REFERENCES

- Bengtsson, L. M., M. Botzet, and M. Esch, 1995: Hurricane-type vortices in a general circulation model. *Tellus*, **47A**, 175–196.
- , —, and —, 1996: Will greenhouse gas induced warming over the next 50 years lead to higher frequency and greater intensity of hurricanes? *Tellus*, **48A**, 57–73.
- Benoit, R., M. Desgagné, P. Pellerin, S. Pellerin, Y. Chartier, and S. Desjardins, 1997: The Canadian MC2: A semi-Lagrangian semi-implicit wide-band atmospheric model suited for fine-scale process studies and simulation. *Mon. Wea. Rev.*, **125**, 2382–2414.
- Boer, G. J., G. M. Flato, and D. Ramsden, 2000a: A transient climate change simulation with greenhouse gas and aerosol forcing: Projected climate change to the 21st century. *Climate Dyn.*, **16**, 427–450.
- , —, M. C. Reader, and D. Ramsden, 2000b: A transient climate change simulation with greenhouse gas and aerosol forcing: Experimental design and comparison with the instrumental record for the twentieth century. *Climate Dyn.*, **16**, 405–425.
- Carillo, A., P. M. Ruti, and A. Nvarra, 2000: Storm tracks and zonal mean flow variability: A comparison between observed and simulated data. *Climate Dyn.*, **16**, 219–228.
- Elsner, J. B., T. Jagger, and X.-F. Niu, 2000: Changes in the rates of North Atlantic major hurricane activity during the 20th century. *Geophys. Res. Lett.*, **27**, 1743–1746.
- Emanuel, K. A., 1987: The dependence of hurricane intensity on climate. *Nature*, **326**, 483–485.
- , 2005: Increasing destructiveness of tropical cyclones over the past 30 years. *Nature*, **436**, 686–688.
- Fischer-Bruns, I., H. von Storch, J. F. González-Rouco, and E. Zorita, 2005: Modelling the variability of midlatitude storm activity on decadal to century time scales. *Climate Dyn.*, **25**, doi:10.1007/s00382-005-0036-1.
- Flato, G. M., and G. J. Boer, 2001: Warming asymmetry in climate change simulations. *Geophys. Res. Lett.*, **28**, 195–198.
- , —, W. G. Lee, N. A. McFarlane, D. Ramsden, M. C. Reader, and A. J. Weaver, 2000: The Canadian Centre for Climate Modelling and Analysis, global coupled model and its climate. *Climate Dyn.*, **16**, 451–467.
- Fyfe, J., 2003: Extratropical Southern Hemisphere cyclones: Harbingers of climate change? *J. Climate*, **16**, 2802–2805.
- Goldenberg, S. B., C. W. Landsea, A. M. Mestas-Nunez, and W. M. Gray, 2001: The recent increase in Atlantic hurricane activity: Causes and implications. *Science*, **239**, 474–479.
- Gray, W. M., 1984: Atlantic seasonal hurricane frequency. Part I: El Niño and 30 mb quasi-biennial oscillation influences. *Mon. Wea. Rev.*, **112**, 1649–1668.
- Hart, R. E., and J. L. Evans, 2001: A climatology of the extratropical transition of Atlantic tropical cyclones. *J. Climate*, **14**, 546–564.
- Henderson-Sellers, A., and Coauthors, 1998: Tropical cyclones and global climate change: A post-IPCC assessment. *Bull. Amer. Meteor. Soc.*, **79**, 19–38.
- Holland, G. J., 1997: The maximum potential intensity of tropical cyclones. *J. Atmos. Sci.*, **54**, 2519–2541.
- Houghton, J. T., Y. Ding, D. J. Griggs, M. Noguer, P. J. van der Linden, X. Dai, K. Maskell, and C. A. Johnson, Eds., 2001: *Climate Change 2001: The Scientific Basis*. Cambridge University Press, 881 pp.
- Kalnay, E., and Coauthors, 1996: The NCEP/NCAR 40-Year Reanalysis Project. *Bull. Amer. Meteor. Soc.*, **77**, 437–471.
- Knippertz, P., U. Ulbrich, and P. Speth, 2000: Changing cyclones and surface wind speeds over the North Atlantic and Europe in a transient GHG experiment. *Climate Res.*, **15**, 109–122.
- Knutson, T. R., and R. E. Tuleya, 1999: Increased hurricane intensities with CO₂-induced warming as simulated using the GFDL hurricane prediction system. *Climate Dyn.*, **15**, 503–519.
- , and —, 2004: Impact of CO₂-induced warming on simulated hurricane intensity and precipitation: Sensitivity to the choice of climate model and convective parameterization. *J. Climate*, **17**, 3477–3495.
- , —, and Y. Kurihara, 1998: Simulated increase of hurricane intensities in a CO₂-warmed climate. *Science*, **279**, 1018–1020.
- , T. L. Delworth, K. W. Dixon, and R. J. Stouffer, 1999: Model assessment of regional surface temperature trends (1949–1997). *J. Geophys. Res.*, **104** (D24), 30 981–30 996.
- , R. E. Tuleya, W. Shen, and I. Ginis, 2001: Impact of CO₂-induced warming on hurricane intensities as simulated in a hurricane model with ocean coupling. *J. Climate*, **14**, 2458–2468.
- Krishnamurti, T. N., R. Correa-Torres, M. Latif, and G. Daughenbaugh, 1998: The impact of current and possibly future sea surface temperature anomalies on the frequency of Atlantic hurricanes. *Tellus*, **50A**, 186–210.
- Lambert, S. J., 2004: Changes in winter cyclone frequencies and strengths in transient enhanced greenhouse warming simulations using two coupled climate models. *Atmos.–Ocean*, **42**, 173–181.
- Landsea, C. W., N. Nicholls, W. M. Gray, and L. A. Avila, 1996: Downward trends in the frequency of intense Atlantic hurricanes during the past five decades. *Geophys. Res. Lett.*, **23**, 1697–1700.
- Lunkeit, F., K. Fraedrich, and S. E. Bauer, 1998: Storm tracks in a warmer climate: Sensitivity studies with a simplified global circulation model. *Climate Dyn.*, **14**, 813–826.
- McTaggart-Cowan, R., J. R. Gyakum, and M. K. Yau, 2001: Sensitivity testing of extratropical transitions using potential vorticity inversions to modify initial conditions: Hurricane Earl case study. *Mon. Wea. Rev.*, **129**, 1617–1636.
- , —, and —, 2003: The influence of the downstream state on extratropical transitions: Hurricane Earl (1998) case study. *Mon. Wea. Rev.*, **131**, 1910–1929.
- Moon, I.-J., I. Ginis, and T. Hara, 2004: Effect of surface waves on

- air–sea momentum exchange. Part II: Behavior of drag coefficient under tropical cyclones. *J. Atmos. Sci.*, **61**, 2334–2348.
- Paciorek, C. J., J. S. Risbey, V. Ventura, and R. D. Rosen, 2002: Multiple indices of Northern Hemisphere cyclone activity, winters 1949–99. *J. Climate*, **15**, 1573–1590.
- Perrie, W., X. Ren, W. Zhang, and Z. Long, 2004: Simulation of extatropical Hurricane Gustav using a coupled atmosphere–ocean–sea spray model. *Geophys. Res. Lett.*, **31**, L03110, doi:10.1029/2003GL018571.
- Ren, X., W. Perrie, Z. Long, J. Gyakum, and R. McTaggart-Cowan, 2004: On the atmosphere–ocean coupled dynamics of cyclones in midlatitudes. *Mon. Wea. Rev.*, **132**, 2432–2451.
- Royer, J.-F., F. Chauvin, B. Timbal, P. Araspin, and D. Grimal, 1998: A GCM study of the impact of greenhouse gas increase on the frequency of occurrence of tropical cyclones. *Climatic Change*, **38**, 307–343.
- Sugi, M., A. Noda, and N. Sato, 2002: Influence of the global warming on tropical cyclone climatology: An experiment with the JMA global model. *J. Meteor. Soc. Japan*, **80**, 249–272.
- Swail, V. R., and A. T. Cox, 2000: On the use of NCEP–NCAR reanalysis surface marine wind fields for a long-term North Atlantic wave hindcast. *J. Atmos. Oceanic Technol.*, **17**, 532–545.
- Tanguay, M., A. Robert, and R. Laprise, 1990: A semi-implicit semi-Lagrangian fully compressible regional forecast model. *Mon. Wea. Rev.*, **118**, 1970–1980.
- Tonkin, H., G. J. Holland, C. W. Landsea, and S. Li, 1997: Tropical cyclones and climate change: A preliminary assessment. *Assessing Climate Change: Results from the Model Evaluation Consortium for Climate Assessment*, W. Howe and A. Henderson-Sellers, Eds., Gordon and Breach, 323–355.
- Trenberth, K. E., 2005: Uncertainty in hurricanes and global warming. *Science*, **308**, 1753–1754.
- Tsutsui, J.-I., 2002: Implications of anthropogenic climate change for tropical cyclone activity: A case study with the NCAR CCM2. *J. Meteor. Soc. Japan*, **80**, 45–65.
- , and A. Kasahara, 1996: Simulated tropical cyclones using the National Center for Atmospheric Research community climate model. *J. Geophys. Res.*, **101**, 15 013–15 032.
- Vitart, F., J. L. Anderson, and W. F. Stern, 1999: Impact of large-scale circulation on tropical storm frequency, intensity, and location, simulated by an ensemble of GCM integrations. *J. Climate*, **12**, 3237–3254.
- Walsh, K., and I. G. Watterson, 1997: Tropical cyclone-like vortices in a limited area model: Comparison with observed climatology. *J. Climate*, **10**, 2240–2259.
- , and J. J. Katzfey, 2000: The impact of climate change on the poleward movement of tropical cyclone-like vortices in a regional climate model. *J. Climate*, **13**, 1116–1132.
- , and B. F. Ryan, 2000: Tropical cyclone intensity increase near Australia as a result of climate change. *J. Climate*, **13**, 3029–3036.
- , K.-C. Nguyen, and J. L. McGregor, 2004: Fine-resolution regional climate model simulations of the impact of climate change on tropical cyclones near Australia. *Climate Dyn.*, **22**, 47–56.
- Webster, P. J., G. J. Holland, J. A. Curry, and H.-R. Chang, 2005: Changes in tropical cyclone number, duration, and intensity in a warming environment. *Science*, **309**, 1844–1846.
- Yoshimura, J., M. Sugi, and A. Noda, 1999: Influence of greenhouse warming on tropical cyclone frequency simulated by a high resolution AGCM. Preprints, *23d Conf. Hurricanes and Tropical Meteorology*, Dallas, TX, Amer. Meteor. Soc., 1081–1084.